Performance of Non-Line of Sight Underwater Optical Wireless Communication Links

A. B. Umar, M. S. Leeson*
School of Engineering, University of Warwick, Coventry, CV4 7AL, UK
mark.leeson@warwick.ac.uk

(Received 04th February, 2020; Accepted 16th March, 2020; Published: 30th March, 2020)

Abstract- Underwater optical wireless communication (UOWC) offers the prospect of higher bandwidths and data rates for underwater communications. However, UOWC systems also suffer from severe absorption and scattering introduced by the underwater channel. They may also be blocked by a myriad of obstructions under the water. Hence, in this paper, we consider the characteristics of a non-line-of-sight (NLOS) UOWC link with multiple scattering based on Monte Carlo simulation. We address the channel response of an NLOS-UOWC system with different channel modulation schemes. The resultant channel impulse (CIR) response varies with the type of water considered and the receiver field of view (FOV). Thus, we investigate the CIR and likely transmission distance for clear ocean, costal water and turbid water for FOV values of 30° and 60°. Then, the CIR obtained using different modulation formats is investigated in coastal water since this is a likely application medium. Finally, we evaluate the bit error rate (BER) and throughput of the system including variation in the receiver bandwidth. It is seen that distances over 80 meters are possible, providing BER values of 10^{-4} or better and throughput of 2.1 Mbps. This demonstrates that NLOS-UOWC offers a route to transmission at higher speeds than incumbent technologies in areas such as inshore environmental monitoring or oil exploration.

Key Words: Non-Line of Sight Communications, Underwater Optical Wireless Communications, Monte-Carlo Simulation, Radiative Transfer Equation.

1. INTRODUCTION

In recent years, there has been a significant increase in study and exploitation of the underwater environment driven by many applications such as oceanography research and offshore oil exploration [1]. Moreover, the emerging Internet of Underwater Things (IoUT) [2] adds to the need for increased wireless data rates and reliability in the underwater environment. The established method for underwater communications is via acoustic waves [3] that have can operate over large distances but offer limited performance because of low bandwidth, high latency, high transmission losses and time-varying multipath propagation. Acoustic underwater communication currently supports data rates of up to hundreds of kbps for a few meters and tens of kbps for a few kilometers [3]. Presently, the increase in the number of unmanned underwater devices such as remotely operated vehicles (ROVs) and autonomous underwater vehicles (AUVs) also produces demands for high capacity and high bandwidth to transfer information underwater.

Advances in visible light technology combined with the low attenuation blue-green wavelength window of seawater have made underwater optical wireless communications (UOWC) a viable and attractive alternative or complementary solution to acoustic communications, offering data rates approaching Gbps, lower latency by virtue of the speed of light, and better security [4]. Despite the wide range of potential applications that could benefit significantly from UOWC, such systems suffer from significant channel absorption and scattering, and may be experience blocking by underwater obstructions.

The majority of UOWC work to date has concentrated on when there is a clear path between the transmitter and the detector, the line-of-sight (LOS) configuration [5], [6]. The work of Hanson and Radic [7] considered single scattering in a LOS configuration to attain a data rate of 1 Gbps, extended to LOS multiple scattering by Gabriel et al. [5] utilizing 100 Mbps. In practical scenarios, LOS communication links are not always possible due to obstructions from sea creatures, bubbles, large suspended particles and features of the seabed, especially in coastal and turbid water environments. LOS links are also unsuitable when the transmitter and receiver are non-stationary nodes [8]. Thus, non-LOS (NLOS) UOWC techniques are needed to fully explore the underwater channel but very little work has been reported so farregardingit. Arnon and Kedar [9] proposed a NLOS UOWC link with single scattering and analyzed the bit error rate (BER) performance. Choudhary et al. [10] reported the determination of impulse responses based on Monte-Carlo (MC) simulation for NLOS UOWC. The same group also carried out a path loss performance analysis [11] for NLOS UOWC with different fields of view for clear ocean water using just on-off keying (OOK) modulation and neglecting receiver noise.

So, to overcome the shortfalls in existing designs we concentrate here on a three-dimensional multiple scattering NLOS UOWC channel, investigating the channel impulse response (CIR) and system performance in different water types using a variable field of view (FOV). The simulation considers the trajectories of a large number of photons using the MC approach for a variety of modulation schemes in the presence of receiver noise. Thus, the contributions of this paper for characterization of NLOS-UOWC are as follows:

i) We employ the established Henyey-Greenstein (HG) phase function in the impulse response model with tracking of photons and scattering that fit well with the MC simulation.
ii) Clear ocean water, coastal water and turbid water are considered.

iii) The CIR characteristics of the channel modulation schemes quadrature phase shift keying (QPSK), 8-PSK 16-quadrature amplitude modulation (16-QAM) and 64-QAM are investigated.
iv) The BER and throughput of the underwater optical NLOS channel are evaluated.

The remainder of this paper is organized as follows. In Section 2, we introduce the model with a block diagram and description of each block. Section 3 presents the details of the model from the implementation methodology to the mathematical framework that shows the effect of seawater on beam pulse propagation and the basic rules of our MC approach. Section 4 covers simulation results and their discussion, with conclusions presented in Section 5.

2. NLOS-UOWC SYSYEM

Characterizing light-water interaction is a highly complicated procedure encompassing the effects when photons meet matter. Fig.1 presents an abstract picture, illustrating the process when light meets a particle within the water causing some photons to be absorbed, some to be transmitted and the trajectory of some others to be altered (scattering).

Such of interactions are part of radiative transfer function (RTF) theory and are called the inherent optical properties (IOPs) of the water [12].In turbid and coastal waters, suspended particles mean that photons will undergo multiple scattering. One of the IOPs is absorption, which is defined as the irreversible loss of a fraction of the incident power of the photon when it interacts with water or with any other particle

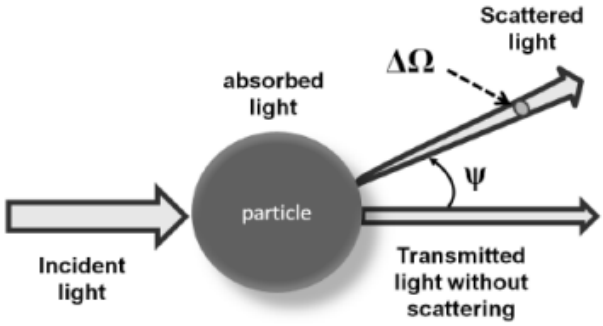

Fig. 1: Underwater optical light-particle interaction.

inside the water. The second IOP is scattering, which is the deflection of photons from their original path when they interact with water and other particles [13]. The attenuation coefficient (also known as the extinction coefficient) defines the total loss of energy as a sum of the absorption coefficient, $a(\lambda)$, and the scattering coefficient, $b(\lambda)$.

$$c(\lambda) = a(\lambda) + b(\lambda) \quad (1)$$

Here, we focus on clear ocean, coastal and turbid water with channel parameters as given in Table 1 [11].

TABLE 1. Absorption, Scattering and Attenuation Coefficient for the four Water Types [11]

Water Type	$a(\lambda)$ (m^{-1})	$b(\lambda)$ (m^{-1})	$c(\lambda)$ (m^{-1})
Clear ocean	0.069	0.08	0.15
Coastal	0.088	0.216	0.305
Turbid	0.295	1.875	2.17

Understanding the statistical distribution of optical signal fluctuations for reliable, efficient, and robust UOWC system design requires detailed modeling and characterization of the

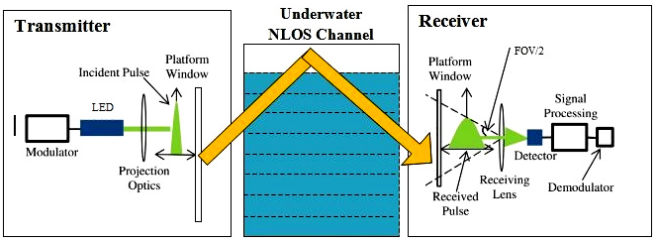

Fig. 2: Schematic block diagram of UWOC-NLOS system.

underwater wireless optical channel. We consider an NLOS–UOWC system with transmitter (TX), receiver (RX), and NLOS channel shown schematically in Fig. 2. In the transmitter section, a light pulse is modulated and enters the medium after passing through appropriate projection optics. Here we consider the underwater channel to be homogeneous and time-invariant given the very high propagation speed of light and small propagation distance. The receiver section consists of a collecting lens which focuses the light incident on it to a photodetector placed at its focal point followed by post-detection signal processing and demodulation.

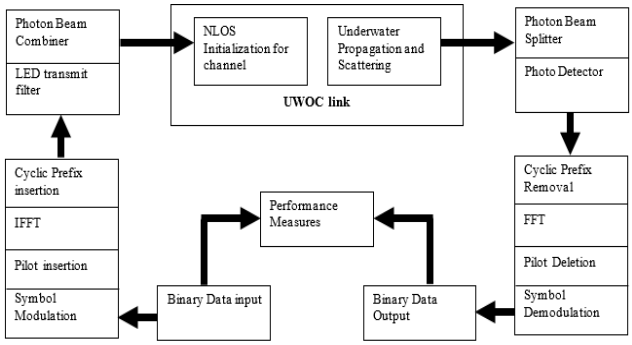

In UOWC, the noise is a combination of background noise, thermal noise, shot noise and dark current noise, which can be approximated and modelled as additive white Gaussian noise (AWGN) [13]. Based on the parameters used here and in [13], the background noise is negligible compared to receiver noise because of the substantial attenuation of the sun underwater so we include only receiver AWGN noise, namely thermal, shot and dark current noise.

3. DETAILS OF THE MODEL

The process flow of our NLOS-UOWC model is shown in Fig. 3. This begins with the generation of a sequence binary data using a random generator, which is the mapped to the appropriate QAM or PSK constellation points to enable performance investigations using different modulation schemes. Following modulation, binary streams become symbols corresponding to the Fourier transform size with auxiliary information inserted using additional pilot symbols. The useful data and the auxiliary data are transformed using the inverse fast Fourier transform (IFFT), before addition of the header and cyclic prefix (CP). Finally, after digital/analog

(D/A) conversion the signals generated are used to drive the LED transmit filter. The photon beam combiner (PBC) collimates the parallel optical signals and combines them into a single beam for transmission through the channel. This signal propagates through the NLOS underwater channel with the aim of enabling stable wireless transmission. In the receiver section, the optical signals that have passed through the underwater channel are converted to parallel signals using the photon beam splitter (PBS) for photodetection. After analog/digital (A/D) processing, symbol synchronization is required. Then, the CP is removed and the signal converted using the fast Fourier transform (FFT) prior to auxiliary symbol removal and demodulation, followed by signal reconstruction for error counting.

A. Photon Angle Scattering

As seen in Section 1, after interaction with a particle, the photon deviates from its incoming direction. The new propagation direction is determined by regenerating randomly the azimuth angleϕ and the scattering angle θ [14]. The angle ϕ is considered as a random variable (RV) uniformly distributed over [0, 2π]. However, the distribution of the scattering angle, θ, has to take account of the medium characteristics, which is achieved via a phase function. Here we use the Henyey-Greenstein (HG) phase function [15] that is commonly employed in ocean optics to model light scattering [16]. This has the form:

$$\beta(\theta) = \frac{1-g^2}{4\pi(1+g^2-2g\cos\theta)^{3/2}} \quad (2)$$

where$g$ is the HG asymmetry parameter that depends on the medium characteristics. To determine g, the average of the cosine of the scattering angle over all scattering directions is determined. That is to say $g = \overline{cos\theta}$, where here we take $g = 0.924$[5]. The probability density function PDF of the scattering phase function is then given by:

$$\rho_{\mathrm{HG}}(\cos\theta, g) = \frac{1-g^2}{2(1+g^2-2g\cos\theta)^{3/2}} \quad (3)$$

This is employed in our NLOS UOWC simulation model that is now described.

B. MC Channel Modelling

We adopt a method describing the photon propagation via a probability distribution that defines the path length of the photon movement before a photon-particle interaction, and the angles of scattering after a scattering event occurs. Since MC is a statistical approach, we calculate the angles and directions for many photons producing an RTE solution method using three steps [11]: (a) initialization of photon properties; (b) photon-particle interaction; (c) photon reception.

Prior to describing the MC steps in detail, we first present the link configuration used, which is shown schematically in in Fig. 4. The transmitter (Tx) and receiver (Rx) are separated by a distance d, and Rx has aperture area A_r. The Tx and Rx are located at (0, 0, 0) and (0, d, 0) respectively, with respective elevation angles θ_{tx} and θ_{tx}. The angle ϕ_{tx} is the transmitter divergence angle and $\phi_{rx}$is the FOV; to locate the beam, initial azimuth angles $\psi_t$and ψ_r respectively are taken; MC simulation [17] captures the life of the photons generated. This begins with generating photons, which are then scattered and positioned with new directional coordinates (ψ, θ)referenced to the current direction after every interaction with water particles until they are lost or received. Losses occur because of every interaction produces some energy reduction. If a photon is received by the Rx, then the receiving probability and the impulse response is calculated, and the process is repeated for all photons.

(i) Initialization of Photon Properties

The initial simulation conditions determine: the starting location in Cartesian coordinates; photon direction using directional cosines of the photons; type of environment to be simulated; nature of the photon source. The projections are defined as:

$$\mu_x = \cos\psi_{ini}\sin\theta_{ini} \quad (4)$$

$$\mu_y = \sin\psi_{ini}\sin\theta_{ini} \quad (5)$$

$$\mu_x = \cos\theta_{ini} \quad (6)$$

Then the scattering azimuth angle, ψ,can be computed using:

$$\psi = 2\pi\xi \quad (7)$$

whereξ is a uniform RV in[0,1].

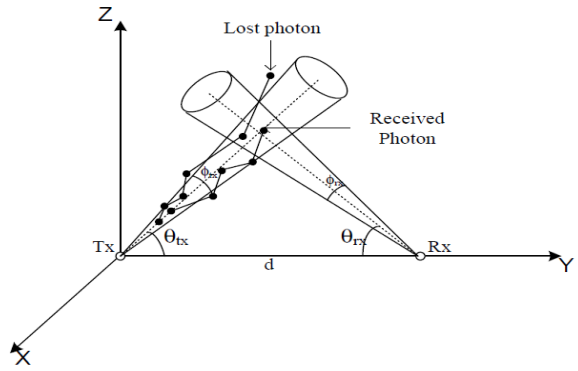

Fig. 4: NLOS UOWC channel link

(ii) Photon-Particle Interaction

The photon travels a random distance, or *step size*, Δs, before interaction with a scattering particle that is given by:

$$\Delta s = -\frac{\log\xi^s}{c(\lambda)} \quad (8)$$

with ξ^s being a uniform random RV also drawn from [0,1].When interacting with the particle, the photon loses a fraction of its initial weight (hereafter referred to asthe weight drop) and deviates from its initial direction (photon scattering) [5]. The photon weights before and after the interaction are denoted by W_{bf} andW_{af}, respectively. Their relationship is:

$$W_{\mathrm{af}} = \left(1-\frac{a(\lambda)}{c(\lambda)}\right)W_{\mathrm{bf}} \quad (9)$$

The trajectory direction of a photon is also randomly changed with the scattering zenith angleθ as a result of the scattering effect. So, to produce a random θ, we initially produce another uniform RV in [0,1], χ_{HG}. This provides an implicit relationship:

$$\chi_{\mathrm{HG}} = \int_0^{\theta} \rho_{HG}(\Theta, g)\sin\Theta\, d\Theta \quad (10)$$

in terms of the dummy variable Θ, from which θ is obtained[5]. The interaction then produces photon coordinates and direction cosines thus:

$$x' = x + \mu_x\Delta s \quad (11)$$

$$y' = y + \mu_y\Delta s \quad (12)$$

$$z' = z + \mu_z\Delta s \quad (13)$$

$$\mu_x' = \mu_x \cos\theta + \frac{\sin\theta}{\sqrt{1-\mu_z^2}}\left(\mu_x\mu_z \cos\psi - \mu_y \sin\psi\right) \quad (14)$$

$$\mu_y' = \mu_y \cos\theta + \frac{\sin\theta}{\sqrt{1-\mu_z^2}}\left(\mu_y\mu_z \cos\psi - \mu_x \sin\psi\right) \quad (15)$$

$$\mu_z' = \mu_z \cos\theta - \sin\theta\sqrt{1-\mu_z^2}\cos\psi \quad (16)$$

(iii) Photon Reception

The process "step size generation, weight drop and angle scattering" described above is repeated until one of the following events happens:

a) The photon weight becomes negligible and it is considered to have been absorbed; the threshold limit is set to 10^{-4} here [5].
b) The photon reaches the receiver plane; if it is within the receiver aperture, it is considered to have been effectively received or else it is considered lost.

4. RESULTS AND DISCUSSION

The model described above for the NLOS UOWC system with channel characteristics utilizing the HG model was run using the MATLAB package with the parameters given in Table 2[11]. We did not include receiver spatial filtering since in deep-sea waters, background radiation is negligible, so the system was subject to AWGN at the receiver. First, we determined the total received NLOS intensity as a function of distance for the three water types specified in Table 1 using a 30° FOV, shown in Fig. 5. The relative intensity is determined

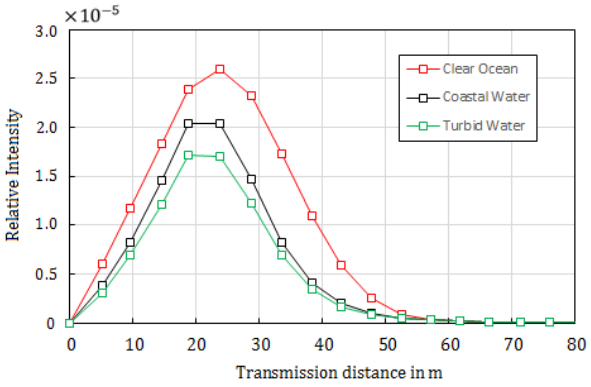

Fig. 5: CIR for the water types in Table 1.

by summing the weight of the photons that arrive in a particular time window and normalizing this with the total transmitted weight (here 10^6 photons). The impact of attenuation and scattering may be observed, particularly at the 50dB loss point (10^{-5} relative intensity).For clear ocean water this occurs at circa 39 meters, whereas for coastal and turbid water the corresponding points are approximately 33 and 31 meters respectively since scattering is more pronounced. Having established the impact of the type of water, we then turned our attention to coastal water, since this is the most likely application scenario of NLOS transmission. Fig. 6 shows the CIR in terms of relative the intensity of the received signal as a function of distance at FOV values of 30° and 60° when employing QPSK, 8-PSK, 16-QAM and 64-QAM. Although these are similar, the highest intensity achieved in our design was when using 64-QAM. Compared with other three modulation schemes, this provided the best receiver CIR

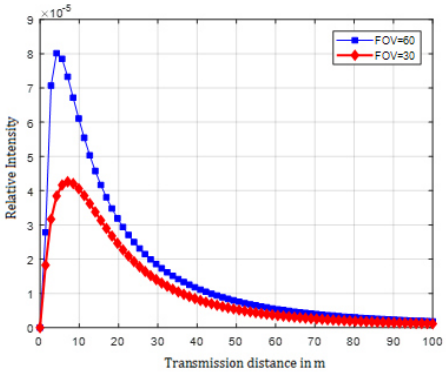

(a) QPSK

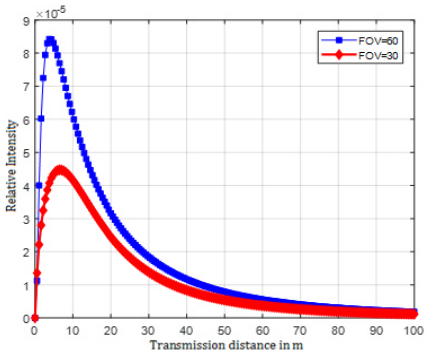

(b) 8-PSK

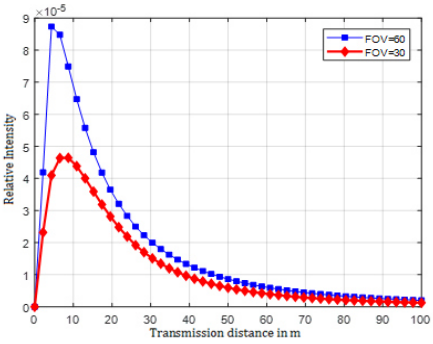

(c) 16-QAM

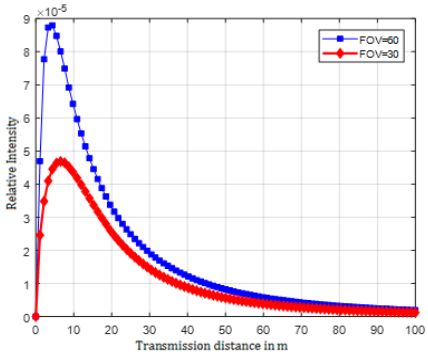

(d) 64-QAM

Fig. 6.: Coastal water CIR curves for various modulation schemes and 30° and 60° FOV values

performance. Thus, based on the CIR results, 64-QAM was adopted to investigate BER and throughput of a complete communication system as a function of the customary ratio of the energy per bit to the noise power spectral density (E_b/N_0)

at the receiver. The analysis was performed for a range of receiver bandwidths from 20 MHz and 420 MHz.

TABLE 2: Simulation parameters and corresponding values [11]

Parameter	Value
Transmission wavelength	532 nm
Elevation angle (θ_t)	$\pi/4$
Elevation angle (θ_r)	$\pi/2$
Divergence angle (ϕ_t)	$\pi/3$
Aperture diameter	20 cm
Range sensitivity	20 m
FOV	$30^{\circ}, 60^{\circ}$
Bitrate	100Mbps
Modulation schemes	QPSK, 8-PSK, 16 QAM, 64 QAM

TABLE 3. Propagation distances for different modulation schemes

Modulation Type	Propagation distance (m)	
	FOV= 30°	FOV= 60°
QPSK	64	72
8-PSK	68	75
16-QAM	71	80
64-QAM	74	83

As shown in Fig. 7, the lowest BER is obtained by using a bandwidth of 20 MHz and the BER increased with bandwidth since the thermal noise at the receiver was proportional to the bandwidth. For a BER of 10^{-4}, at 20MHz the sensitivity was 23.2dB whereas this increased to 24.3 dB when using a 420MHz bandwidth.

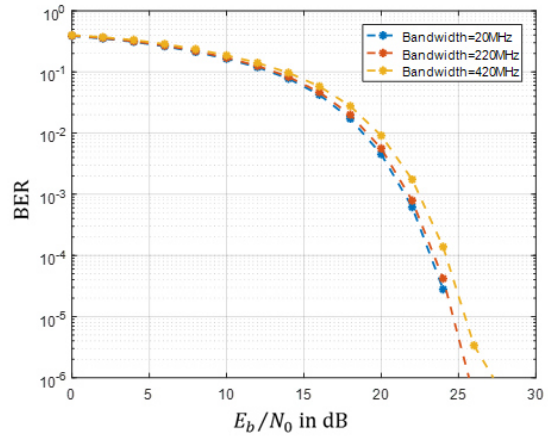

Fig. 7: BER of NLOS UOWC using 64-QAM.

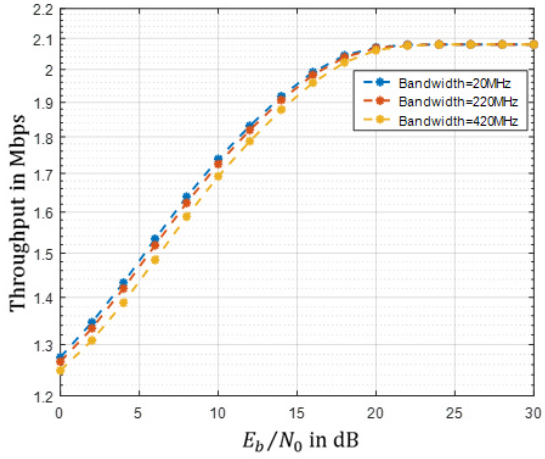

Fig. 8: Throughput of NLOS UOWC using 64-QAM.

Fig. 8, shows the system throughput results as a function of E_b/N_0. As would be expected, this increases with E_b/N_0 as the level of the signal relative to the noise improves. The bandwidth has only a small effect, becoming negligible for E_b/N_0 greater than approximately 20 dB. At this point, the throughput tends to the maximum value of 2.1 Mbps observed at $E_b/N_0 = 30$ dB.

5. CONCLUSION

We have presented the details of and results from a simulation of the characteristics of a NLOS-UOWC transmission system. Using MC simulation based on the RTE, we have incorporated the effects of losses due to absorption, scattering, and attenuation in NLOS-UOWC links. The scattering is accommodated utilizing the commonly employed HG function. Initially, we have characterized the CIR for clear ocean, coastal water and turbid water to ensure that our simulation was producing realistic results. We then focused our attention on the impact of FOV for different modulation schemes in coastal waters, since these represent a likely environment for NLOS-UOWC applications as we acknowledge that clear ocean admits the use of LOS systems, with turbid water offering similar but inferior performance to coastal water. The results demonstrate that using a 30° FOV, transmission distances range from 64 meters using QPSK to 74 meters employing 64-QAM. For 60°, the corresponding distances are 72 meters and 83 meters for the same modulation schemes. The receiver bandwidth was found to have a relatively modest impact when varied from 20 MHz to 420 MHz, producing a maximum power penalty of 1.1 dB for the largest value. In terms of throughput, using a 100 Mbps transmission rate produced 2.1 Mbps over the channel because of its highly lossy nature. Nevertheless, it is possible to communicate at BER values that would enable the use of forward error correction to deliver highly reliable communication over useful distances. This also opens up the prospect of further work to develop an NLOS-UOWC system with multiple input and multiple output (MIMO) transmission.

REFERENCES

[1] E. Felemban, F. K. Shaikh, U. M. Qureshi, A. A. Sheikh and S. B. Qaisar, "Underwater Sensor Network Applications: A Comprehensive Survey," *Int. J. of Dist. Sen. Net.*, vol. 2015, art. 896832, 14 pages, 2015.

[2] M. C. Domingo, "An overview of the internet of underwater things," *J. of Net. and Comp. Appl.,* vol. 35, no. 6, pp. 1879–1890, 2012.

[3] I. F. Akyildiz, D. Pompili and T. Melodia, "Underwater acoustic sensor networks: research challenges," *Ad Hoc Networks,* vol. 3, no. 3, pp. 257-279, 2005.

[4] P. Lacovara, "High-Bandwidth Underwater Communications," *Marine Tech. Soc. J.,* vol. 42, no. 1, pp. 93-102, 2008.

[5] C. Gabriel, M. Khalighi, S. Bourennane, P. Lon, and V. Rigaud, "Monte Carlo-Based Channel Characterization for Underwater Optical Communication Systems," *J. Opt. Commun. Netw. vol. 5, no. 1,* pp.1-12, 2013.

[6] S. Tang, Y. Dong, and X. Zhang, "On link misalignment for underwater wireless optical

communications," *IEEE Commun. Letts,* vol. 16, no. 10, pp 1688-1690, 2012.

[7] F. Hanson, and S. Radic, "High bandwidth underwater optical communication," *In Appl. Opt*., vol. 47, no. 2, pp. 277-283, Jan. 2008.

[8] L. J. Johnson, F. Jasman, R. J. Green, and M. S. Leeson, "Recent advances in underwater optical wireless communications," *Underwater Tech.*, vol. 32, no. 3, pp. 167–175, 2014.

[9] S. Arnon, and D. Kedar, "Non-line-of-sight underwater optical wireless communication network" *J. Opt. Soc. Am. A,* vol. 26, no. 3, pp. 530-539, 2009.

[10] A. Choudhary, V. K. Jagadeesh, and P. Muthuchidambaranathan, "Pathloss analysis of NLOS underwater wireless optical communication channel," in Proc. Int. Conf. Electron. Commun. Syst. (ICECS), IEEE Press, Feb. 2014, 4 pp. doi: 10.1109/ECS.2014.6892620.

[11] V. K. Jagadeesh, A. Choudhary, F. M. Bui, and P. Muthuchidambaranathan, "Characterization of Channel Impulse Responses for NLOS Underwater Wireless Optical Communications," in Proc. International Conference on Advances in Computing and Communications (ICACC), IEEE Press, Aug. 2014 IEEE, pp. 77-79, doi: 10.1109/ICACC.2014.24.

[12] C. D. Mobley, Light and Water: Radiative Transfer in Natural Waters, 1st ed. San Diego: Academic, pp. 60-144, 1994.

[13] H. M. Oubei et. al., "2.3 Gbit/s underwater wireless optical communications using directly modulated 520 nm laser diode," *Opt. Exp.*, vol. 23, no. 16, pp. 20743-20748, 2015.

[14] S. K. Sahu, and P. Shanmugam, "A theoretical study on the impact of particle scattering on the channel characteristics of underwater optical communication system," *Opt. Comm.*, vol 408, pp. 3-14, 2018.

[15] L. C. Henyey and J.L. Greenstein, "Diffuse radiation in the galaxy," Astrophys. J., vol. 93, pp. 70-83, 1941.

[16] T. Harmel et. al., "Laboratory experiments for inter-comparison of three volume scattering meters to measure angular scattering properties of hydrosols," *Opt. Exp.*, vol. 24, no. 2, pp. A234-A256, 2016.

[17] J. Huang, Y. Zhang, D. Li, and S. Ren, "Analyzation and Simulation of Underwater Laser Communication Based on Monte Carlo Mechanism," Proc. 7th International Conference on Intelligent Human-Machine Systems and Cybernetics, IEEE Press, Aug. 2015, vol. 2, pp. 517-520, doi:10.1109/IHMSC.2015.252.